Chinese Chemical Letters 34 (2023) 108201

Contents lists available at ScienceDirect

Chinese Chemical Letters

journal homepage: www.elsevier.com/locate/cclet

Indocyanine green-/TLR7 agonist-constructed thermosensitive liposome for low-temperature PTT induced synergistic immunotherapy of colorectal cancer

Xiang Sun[a], Yanmin Wang[a], Tao Du[a], Qiang Zhang[a], Shuo Li[b], Qinda Chen[c], Miao Wang[a,*], Xiumin Wang[c], Lei Ren[a,d,*], Xueqin Zhao[b,*]

[a] Department of Biomaterials, Higher Educational Key Laboratory for Biomedical Engineering of Fujian Province, Research Center of Biomedical Engineering of Xiamen, College of Materials, Xiamen University, Xiamen 361005, China
[b] Zhejiang Provincial Key Laboratory of Silkworm Bioreactor and Biomedicine, College of Life Science and Medicine, Zhejiang Sci-Tech University, Hangzhou 310018, China
[c] School of Pharmaceutical Sciences, Xiamen University, Xiamen 361102, China
[d] State Key Laboratory of Physical Chemistry of Solid Surfaces, College of Chemistry and Chemical Engineering, Xiamen University, Xiamen 361005, China

ARTICLE INFO

Article history:
Received 4 October 2022
Revised 1 February 2023
Accepted 8 February 2023
Available online 10 February 2023

Keywords:
Colorectal cancer
Liposomes
Photothermal therapy
Immunotherapy
Indocyanine green

ABSTRACT

Colorectal cancer (CRC) is a lethal malignancy with a high mortality rate due to its low immunogenicity, the strong immunosuppressive milieu and poor drug permeability. To overcome these obstacles, a cascade synergistic nanosystem (denoted as R837/ICG@Lip) was developed *via* self-assembly of heater indocyanine green (ICG) and toll-like receptor-7 agonist imiquimod (R837) into thermosensitive liposome for simultaneous induction of immunogenic cell death (ICD) and reversing of suppressive tumor microenvironment. The obtained nanoparticles exhibited NIR-triggered drug release, good photothermal conversion efficiency and phototoxicity towards CT26 colorectal cancer cells. *In vivo* results reveal that the R837/ICG@Lip could be effectively accumulated in CT26 subcutaneous tumors and the draining lymph nodes. More importantly, R837/ICG@Lip-mediated low-temperature photothermal therapy triggers ICD, promotes the maturation of host dendritic cells (DCs), and subsequently amplifies adaptive antitumor T-cell responses, resulting in 'Cold to Hot' transition. Besides directly affecting immune cells, the secretion of some immune-related cytokines further indirectly boosted anti-cancer immunity. After combining with the indoleamine 2,3-dioxygenase (IDO) inhibitor, the systemic antitumor immune response was further augmented, achieving best tumor inhibition effects. Thus, low-temperature mediated photoimmunotherapy targeting multiple antitumor immune pathways boost synergistic antitumor immunity of tolerance tumors.

Colorectal cancer (CRC) is the third most common malignant tumor worldwide [1]. The antitumor cellular immunity is initiated by the release of tumor-associated antigens (TAAs), then delivered by antigen-presenting cells (APCs), resulting in T cell-mediated cellular immunity [2]. Nanoparticle (NP)-assisted photothermal therapy (PTT) is an effective treatment method by hyperthermia-induced apoptosis or necrosis of cancer cells [3]. PTT induced tumor cell residues could serve as endogenous tumor antigens and elicit tumor-specific antigen-based responses [4,5], thus reducing the large heterogeneity of individual tumors compared with traditional subunit vaccine. Unfortunately, high levels of hyperthermia ($\geq$50 °C) induced undesirable local inflammation and thermal damage to adjacent healthy cells and the immune antigens due to unavoidable heat diffusion, resulting in less TAAs release and inadequate APCs activation. Low-temperature ($<$50 °C) photothermal therapy (LT-PTT) was reported to not only directly damage cancer cells with mild toxicity to normal tissues, but also improve anti-tumor immunity by modulating the local tumor microenvironment such as the partial disruption of extracellular matrix, the decrease of interstitial fluid pressure, and the increase of the blood perfusion [6–8]. However, the antitumor immune response caused by LT-PTT alone is not enough to reverse the immunosuppressive tumor microenvironment (ITM) [9,10]. Considering that dysfunctional DCs would induce antigen-specific immunotolerance [11], extensive works have been carried out to improve maturation of DCs using immunoadjuvants such as toll-like

* Corresponding authors.
E-mail addresses: miaowang@xmu.edu.cn (M. Wang), renlei@xmu.edu.cn (L. Ren), zhaoxueqin@zstu.edu.cn (X. Zhao).

https://doi.org/10.1016/j.cclet.2023.108201
1001-8417/

receptor (TLR) agonists [6,7,12]. TLRs work as pattern recognition receptors, and response to damage-associated molecular patterns or pathogen-associated molecular patterns, inducing an innate immune response [13]. As toll-like receptor-7 (TLR-7) agonist, Imiquimod (R837) can significantly promote the DCs maturation, elicit the initiation of tumor-specific T cells and upregulate co-stimulating molecules [14–20]. Studies suggested R837 can stimulate DC activation in PTT-synergized immuno-oncotherapy to further strengthen the immunogenic cell death (ICD) response [21]. However, PTT-induced therapeutic efficacy of cold tumors severely limited by immunosuppressive tumor microenvironment [2,22,23].

Indoleamine 2,3-dioxygenase (IDO) is an important immunosuppressive enzyme, which prevents $CD8^+$ T cell priming by catalyzing the oxidative catabolism of tryptophan (TRP) to kynurenine. IDO-induced ITM displays moderate tolerance to apoptotic cells, thus weakens, the therapeutic effect of ICD [4]. In addition, IDO-expressing cells deplete TRP and induce T-cell apoptosis. The administration of R837 and simultaneous inhibition of IDO activity promoted the tumor antigen-specific response and inhibited tumor growth *in vivo* [24]. Immunotherapy based on immune checkpoint inhibitors (ICIs), such as anti-PD-1 therapy, has been proven to be a promising paradigm for cancer treatment [25]. However, it has a limited therapeutic efficacy to the majority of CRC patients due to insufficient T-cell infiltration of cold tumors [2,22,23]. In this scenario, combination therapy to target both promotion of tumor immunogenicity and induction of $CD8^+$ T cell infiltration will be required for maximal IDO blockade therapy [26]. So far, the individual and combined impact of PTT, TLR activation, and IDO blockade in tumor-bearing mice has been shown to enhance antitumor effect [11], while the impact of simultaneously targeting all three pathways in tumor-bearing mice is less investigated until now [27]. Zhang *et al*. mixed photothermal agent IR820 loaded nanoparticles (NPs) and 1-MT (IDO inhibitor)-R837 co-loaded ZIF-8 NPs, which sharply suppressed the tumor growth [27]. It is highly desirable to maximize PTT-based anticancer efficiency at a mild temperature.

To achieve better antitumor effect, our research focuses on a low-temperature cancer combination treatment *via* simultaneously targeting promotion of TAAs, DCs activation and induction of $CD8^+$ T cell infiltration. We developed a multimodal nanotherapeutic agents by the self-assembly of photothermal agent indocyanine green (ICG) and TLR-7 agonist R837 into PEGylated thermosensitive liposome for synergistic immune amplification in tumor-bearing mice. Under NIR irradiation, local hyperthermia produced a photothermal ablation effect on tumor tissues and subsequently released TAAs, facilitating DC maturation with R837. Combined with the IDO inhibitor NLG919, the systemic antitumor immune response was further augmented, achieving best tumor inhibition effects.

Following the design above, thermosensitive R837/ICG@Lip liposomes were stably self-assembled *via* the thin-film dispersion method, and then combined sonication and extrusion for a uniform size. The R837/ICG@Lip NPs were individually dispersed as spherical vesicles with the size of 158.7 ± 12.6 nm, as shown in the transmission electron microscopy images (Figs. 1a and b). The successful loading ICG was demonstrated by fluorescence and UV–vis spectrum. Free ICG had characteristic absorption peaks at 714 and 778 nm. Broad NIR absorbance was observed for R837/ICG@Lip NPs at 700–900 nm, and typical peaks were located at 718 and 782 nm from ICG within the liposomes. The loading of R837 on R837/ICG@Lip induced strong UV absorption at 230 nm, which was nearly three times higher than that of ICG due to the superposition of the absorption peaks (Figs. 1c and d). Liposomes are characterized by their heat flux distribution in the range of 30–80 °C. Bare liposome has two peaks at 45.7 and 68.7 °C (Fig. 1e), while the phase transition temperature (T_m) of R837/ICG@Lip elevated slightly to 47.8 °C. The loading efficiency of R837/ICG@Lip was 8.0% for R837 and 8.8% for ICG, which was equivalent to an R837/ICG molar ratio of 1:2.9 (Fig. 1f). When the R837/ICG@Lip was incubated at 37 °C for 60 min, only 25.50% of R837 was released, while after treating with hyperthermia (48 °C), 70.59% of R837 was released within 60 min (Fig. 1g), suggesting temperature sensitive release profile of R837 from liposome (Fig. 1g and Fig. S1 in Supporting information).

The photothermal profile of R837/ICG@Lip was investigated by monitoring temperature changes during 808 nm laser irradiation. As shown in Fig. 1h, laser explosion induced temperature rising by 20 °C due to photothermal effects of ICG, while as control, a negligible temperature increase was observed for PBS solution within the same irradiation time. These results suggested that photothermal conversion of ICG was successfully realized under NIR irradiation, and the use of liposome vehicles did not influence the inherent photothermal conversion efficiency of ICG. Moreover, the temperature rate of increase and final temperature of R837/ICG@Lip exhibited both concentration- and time-dependencies (Fig. 1h). The rate of the temperature increase slowed when the concentration decreased. Notably, R837 burst-like release from R837/ICG@Lip could be repeatedly triggered by NIR laser (Fig. 1i). It is suggesting its great potential in photothermal triggered drug release and PTT based-combination therapy.

To investigate the effects of R837/ICG@Lip on cellular uptake, CT26 cells were co-incubated with R837/ICG@Lip and free ICG for 4 h, respectively. As shown in Figs. 2a and c, all cells displayed bright red intracellular fluorescence. However, R837/ICG@Lip exhibited more red fluorescence signals inside the cells, especially in the nucleus region, indicating that R837/ICG@Lip can greatly promote CT26 cell uptake due to the good affinity of lipids for the cytoplasmic membrane. Moreover, cell internalization was time-dependence (Figs. 2b and d). Blue fluorescence from Hoechst 33342 for cell nucleus staining and red fluorescence from ICG were simultaneously observed in CT26 cells at 0 h, suggesting the fast diffusion and efficient initialization of R837/ICG@Lip into cells. Red fluorescence signals inside the cells were gradually enhanced with incubation, suggesting time-dependent uptake.

To investigate the photokilling effects, the cell viability was evaluated after incubation with R837/ICG@Lip for 24 h. Over 75% viability was maintained even at a high concentration of 100 μg/mL, indicating good cytocompatibility without NIR irritation (Fig. 2e). Upon exposure to the NIR laser, cell viability remarkably decreased to 48.7%, which is a hallmark of PTT-induced cell death. In contrast, free ICG exhibited approximately 50% cell viability at high concentration of 100 μg/mL, which is consistent with previous reports [28,29]. The dark toxicity of ICG may be due that ICG is unstable in aqueous medium of cytoplasm and decomposes into toxic waste materials [29]. Moreover, slightly higher photothermal killing (51.3%) of R837/ICG@Lip was observed compared to that of free ICG (48.8%) in the laser group, which may be due to the high accumulation of R837/ICG@Lip in CT26 cells. In addition, the PTT efficacy of R837/ICG@Lip was dose dependent (Fig. 2f). At a concentration of 10 μg/mL, 75.91% of the cells survived. In comparison, cell viability dropped significantly to 18.13% at the 200 μg/mL concentration. Therefore, R837/ICG@Lip was intrinsically cytocompatible and suitable for PTT. These results also indicated that a low dose of photosensitizer loading had no obvious cytotoxicity to cells [30].

In vivo photothermal effect of R837/ICG@Lip was assessed in CT26 tumor-bearing BALB/c mice after 6 h of administration (Fig. 3a). On 808 nm laser irradiation, the NP-treated tumor temperature rose rapidly and reached 45 °C within 6 min at the therapeutic site, higher than the damage threshold value (42 °C). As control, temperature of PBS was almost unchanged (Fig. 3b). These results confirmed that R837/ICG@Lip resulted in precise *in vivo* photothermal effects.

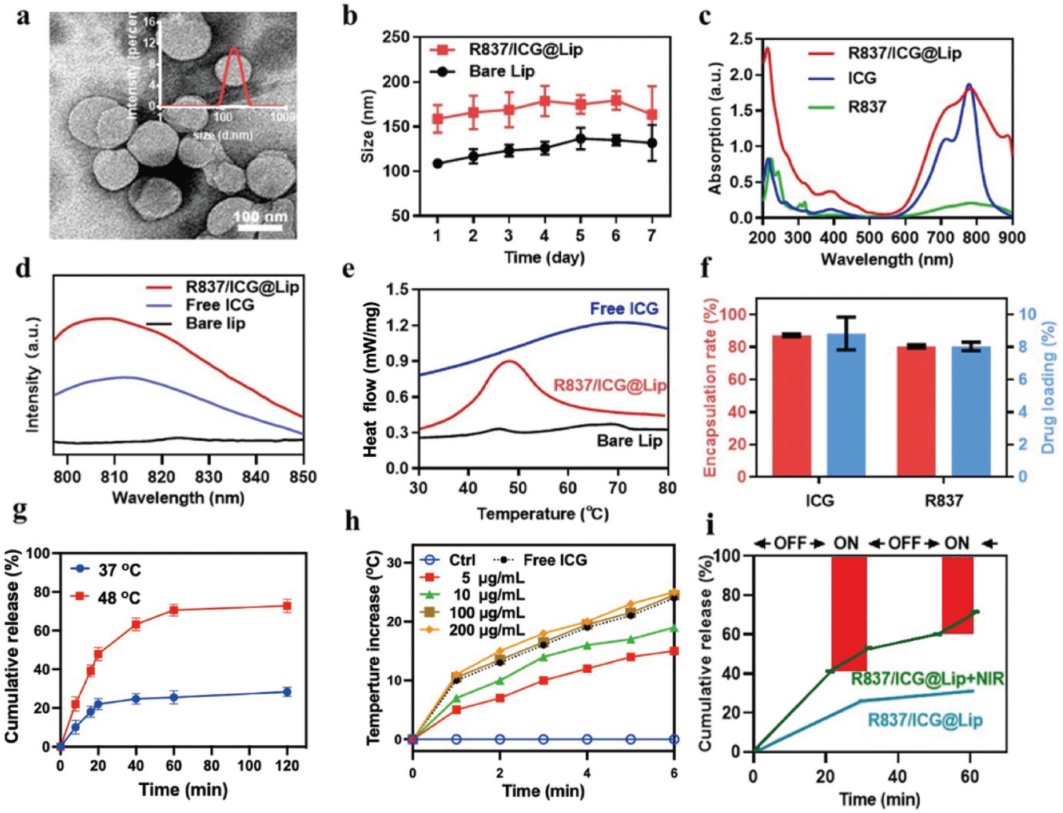

Fig. 1. (a) Transmission electron microscopy of R837/ICG@Lip Nps and its size distribution (inset). Scale bar: 100 nm. (b) The size change curves of R837/ICG@Lip Nps and bare Lip Nps in PBS. (c) UV analysis of R837/ICG@Lip, ICG and R837. (d) Fluorescence spectrum of bare Lip, free ICG and R837/ICG@Lip. (e) Differential scanning colorimeter curve (DSC) of bare Lip, free ICG and R837/ICG@Lip. (f) Encapsulation rate and drug loading of ICG and R837 in R837/ICG@Lip Nps. Time-temperature curve of free ICG and R837/ICG@Lip (g) and (h) R837/ICG@Lip solutions with different concentrations under laser irradiation (808 nm, 1 W/cm^2). (i) R837 Release from R837/ICG@Lip dispersions (100 μg/mL) with or without NIR laser (808 nm, 1 W/cm^2, 10 min) at 30, 60 min, respectively.

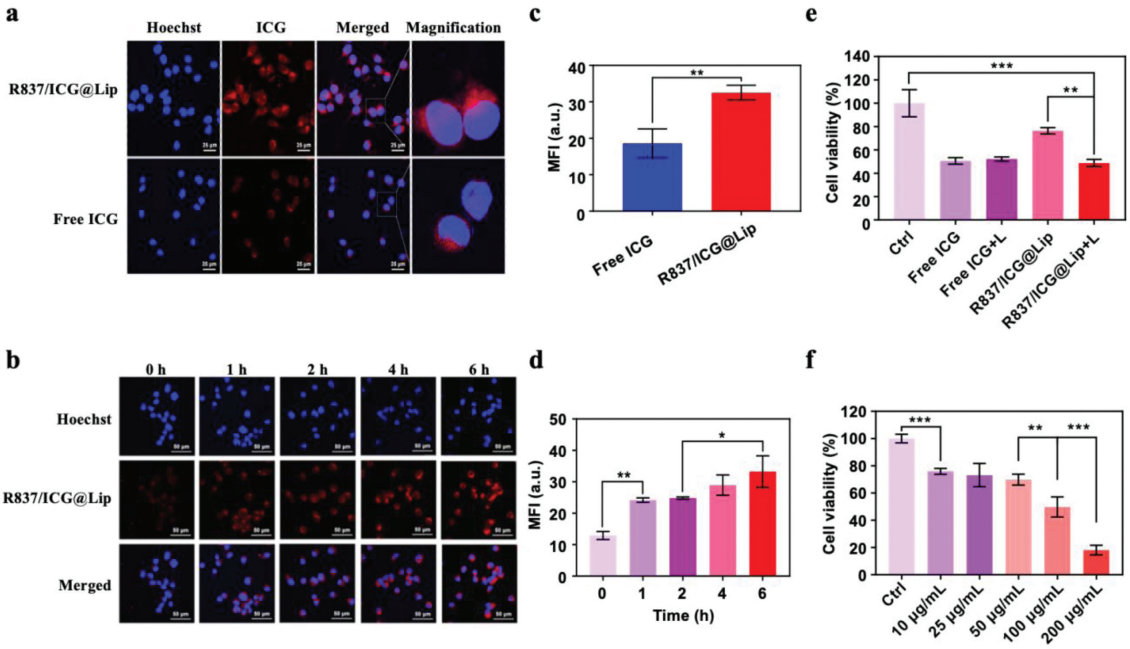

Fig. 2. Confocal images for different groups of CT26 tumor cells with different samples (a) and different time (b) indicated after NIR light irradiation. Scale bars: 25 μm (a), 50 μm (b). (c and d) represented statistical results of the mean fluorescent intensity of (a) and (b) respectively. Cell viability of CT26 cells in different treatment groups indicated (e) with or without laser irradiation and (f) with different concentrations of R837/ICG@Lip under 808 nm laser irradiation. The error bars indicate means ± SD and $n = 5$. $^{*}P < 0.05$, $^{**}P < 0.01$, $^{***}P < 0.001$.

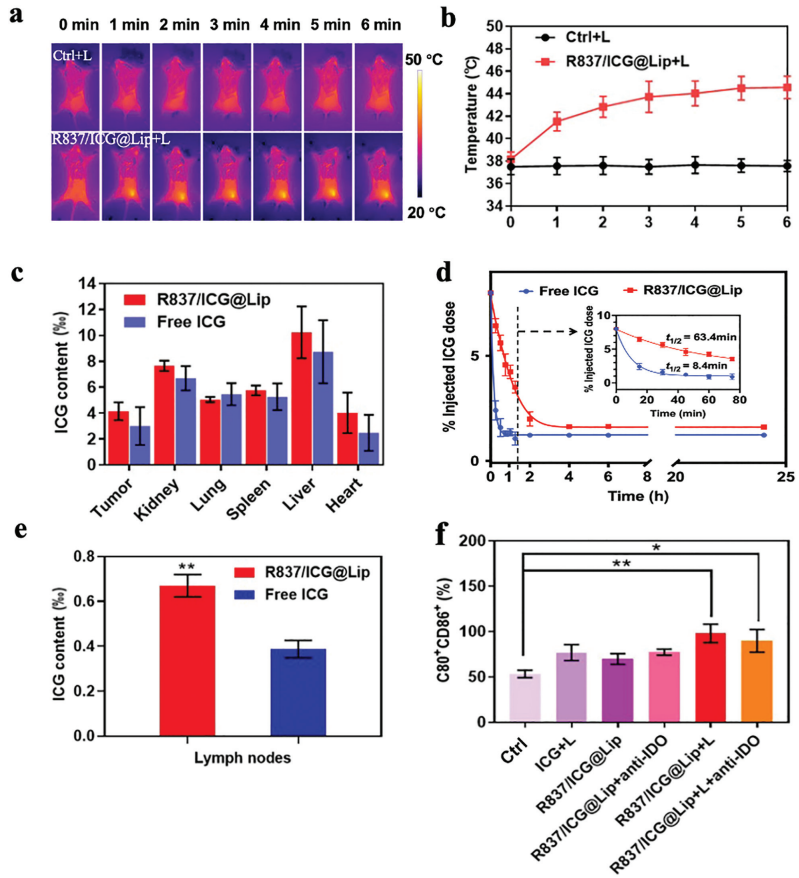

Fig. 3. (a) Infrared thermal images tumor-bearing mice after 6 min of injection with saline and R837/ICG@Lip and (b) corresponding temperature curves at tumor site. (c) Biodistribution profiles and (d) blood circulation of R837/ICG@Lip and free ICG within 24 h (Inset: blood clearance behaviors of R837/ICG@Lip and free ICG within 75 min). (e) ICG and R837/ICG@Lip in lymph nodes. (f) The percent of DC mature detected by FCM. The irradiation conditions are 6 min, 808 nm NIR, and 1 W/cm^2. The error bars indicate means ± SD and $n = 3$. $^*P < 0.05$, $^{**}P < 0.01$.

Distribution of nanoparticles in tumors is essential for specific cancer therapies. Owing to the imaging capability of ICG, the biodistribution of R837/ICG@Lip was investigated by the quantitative analysis of the ICG fluorescence signal. As shown in Fig. 3c, the accumulation of R837/ICG@Lip in the tumor site at 24 h post injection significantly increased by 50.78% when 38.18‰ of injected R837/ICG@Lip remained *in vivo*, 14.30% higher than that of free ICG (32.72‰ of received doses). Moreover, the use of PEGylated liposome significantly improved blood circulation behavior of ICG. Half-life ($t_{1/2}$) of ICG significantly prolonged from 8.4 min to 63.4 min (Fig. 3d). Considering that fast blood clearance of free ICG, data of the drug concentrations within 75 min were extracted and logarithm C_t/C_0 was plot *vs.* time [31,32]. The extremely high correlation coefficients ($R^2 > 0.997$) showed clearance kinetics corresponded with the first-order kinetics (Fig. S2b in Supporting information). Tissue accumulation concentrations of NPs was in the order of liver > kidney > spleen > lung > tumor > heart (Fig. 3c), indicating that the reticuloendothelial system may be involved in the metabolism of R837/ICG@Lip. It is crucial for effective cancer vaccine efficacy to accumulate at lymph nodes (LN) where the maturity of DCs, antigen presentation, and T-cell responses occur. Notably, R837/ICG@Lip exhibited a 1.7-fold higher accumulation in draining lymph nodes than free ICG (Fig. 3e). To verify the DC maturation, the lymph nodes cells were harvested and analyzed. As shown in Fig. 3f, compared with PBS group, R837 led to the improvement in the values of DC mature, consistent with previous reports [33]. On explosion to NIR, the percentage of matured DCs could highly outperformed the counterparts from the case of utilizing a single PTT (ICG+L) or immune activation (R837/ICG@Lip+anti-IDO), suggesting DCs activation *in vivo*.

The *in vivo* therapeutic efficacy of R837/ICG@Lip was heterogeneity (Fig. 4a). Relevant animal experiments have been approved by the Institutional Animal Care and Use Committee of Xiamen University (No. XMULAC20180003). In addition, R837/ICG@Lip, together with TLR agonists (blue curve), showed an increase of 45.7% in tumor ablation, which may be due to the increased secretion of pro-inflammatory cytokines. As expected, LT-PTT based on R837/ICG@Lip, together with TLR-7 agonists, showed the best inhibition of tumor growth with small individual differences (Figs. 4b and c, Fig. S3 in Supporting information). In addition, no significant body weight loss was observed during therapy (Fig. S4 in Supporting information), indicating low systemic toxicity of the different formulations. The moderate weight gain observed in the mice could be ascribed to tumor growth. To further confirm the therapeutic effects and biosafety profile of R837/ICG@Lip *in vivo*, isolated tumors and main organs in different treatment groups were excised on day 14 post administration and examined by immunohistochemical analysis. As shown in Fig. 4d, no obvious organ damage was observed. The highest apoptosis (TUNEL assay) and calreticulin (CRT) expression (CRT assay) occurred in mice treated with R837/ICG@Lip+anti-IDO+L, demonstrating effective ICD *in vivo* induced by NIR-mediated synergistic therapy (Fig. 4e and Fig. S5 in Supporting information). Compared with the normal saline group, significant increase in the densities of CD3$^+$ T, CD45$^+$ T and CD8$^+$ T suggests that synergistic therapy could increase tumor lymphocyte infiltration and induce strong cellular immune response in a mouse model (Fig. 4f and Fig. S6 in Supporting information).

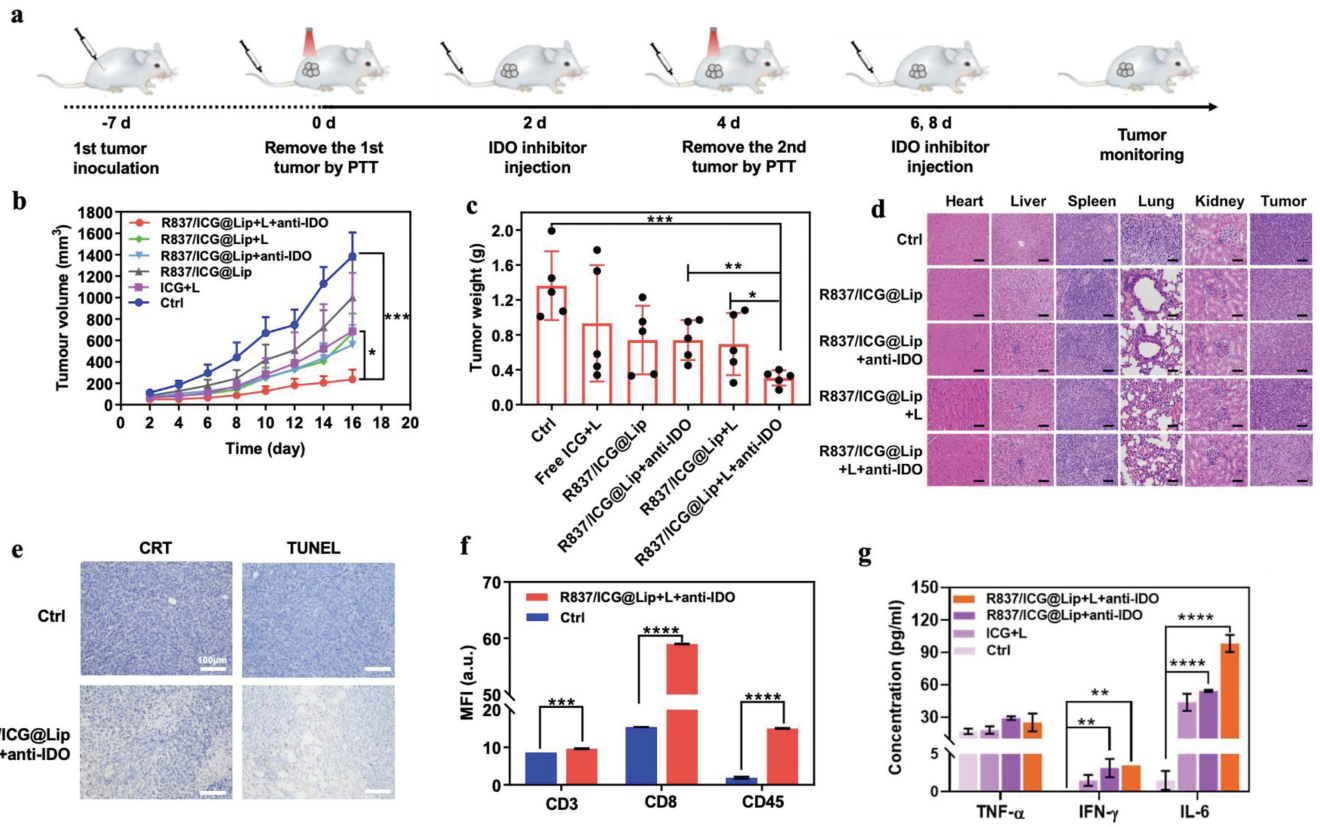

Fig. 4. (a) Administration diagram of R837/ICG@Lip *in vivo*. (b) Tumor growth curve in different treatment groups. (c) Tumor weight in different treatment groups after sacrifice. (d) H&E sections in each treatment group (scale bar: 100 μm). (e) CRT and TUNEL expression in tumors by immunochemistry (scale bar: 100 μm). (f) The mean fluorescent intensity of immunochemistry staining of $CD3^+$ T, $CD8^+$ T cells and $CD45^+$ T cells in tumors. (g) Intratumoural IL-6 and IFN-γ determined by ELISA. The irradiation conditions are 6 min, 808 nm NIR, and 1 W/cm^2. The error bars indicate means ± SD and $n = 5$. $^{**}P < 0.01$, $^{***}P < 0.001$, $^{****}P < 0.0001$.

Besides, the highest expression increment of the inflammatory chemokines was observed (Fig. 4g). These findings clearly demonstrated that R837/ICG@Lip-meditated LT-PTT efficiently and safely boosted systemic immunity to destroy the remaining tumor cells, due to the synergistic effects of TAAs generated from LT-PTT, mature DCs promoted by R837 adjuvant, and the immunoregulation tailored *via* ICI, anti-IDO NLG919.

In conclusion, R837/ICG@Lip with a uniform particle size and high entrapment efficiency was prepared for low-temperature photothermal-immunotherapy. *In vitro* experiments showed that R837/ICG@Lip had a good photothermal conversion effect and significant photo-toxicity in CT26 cells. *In vivo* studies confirmed that R837/ICG@Lip can effectively accumulate in the draining lymph nodes and CT26 subcutaneous tumors, exhibiting a significant synergistic antitumor effect. More importantly, after combining with IDO inhibitor, the systemic antitumor immune response was further augmented, achieving best tumor inhibition effects. Therefore, the R837/ICG@Lip has the therapeutic advantages of non-invasiveness, high bioavailability, and synergistic gain and shows great application potential in the treatment of CRC.

Declaration of competing interest

The authors declare that they have no known competing financial interests or personal relationships that could have appeared to influence the work reported in this paper.

Acknowledgments

This work was supported by the National Natural Science Foundation of China (Nos. 32271469 and U1904206), Fujian Provincial Science and Technology Cooperation Project (No. 20210002), Zhejiang Provincial Natural Science Foundation of China (No. LY18C100002).

Supplementary materials

Supplementary material associated with this article can be found, in the online version, at doi:10.1016/j.cclet.2023.108201.

References

[1] H. Sung, J. Ferlay, R.L. Siegel, et al., CA Cancer J. Clin. 71 (2021) 209–249.
[2] P. Xu, F. Liang, Int. J. Nanomed. 15 (2020) 9159–9180.
[3] J. Yan, C. Wang, X. Jiang, Y. Wei, et al., Int. J. Biol. Sci. 17 (2021) 1361–1381.
[4] L. Fu, X. Ma, Y. Liu, Z. Xu, Z. Sun, Chin. Chem. Lett. 33 (2022) 1718–1728.
[5] P.B. Balakrishnan, E.E. Sweeney, A.S. Ramanujam, R. Fernandes, Int. J. Hyperth. 37 (2020) 34–49.
[6] X. Liu, Q. Su, H. Song, et al., Biomaterials 275 (2021) 120921.
[7] P.M. Chen, W.Y. Pan, C.Y. Wu, et al., Biomaterials 230 (2020) 119629.
[8] X. Yi, Q.Y. Duan, F.G. Wu, Research 2021 (2021) 9816594.
[9] X. Deng, Z. Shao, Y. Zhao, Adv. Sci. 8 (2021) 2002504.
[10] X. Huang, Y. Lu, M. Guo, S. Du, N. Han, Theranostics 11 (2021) 7546–7569.
[11] S. Zuo, J. Song, J. Zhang, et al., Theranostics 11 (2021) 7471–7487.
[12] L. Luo, X. Wang, Y.P. Liao, C.H. Chang, A.E. Nel, ACS Nano 16 (2022) 13168–13182.
[13] B. Zhou, J. Liu, M. Lin, J. Zhu, W.R. Chen, Coord. Chem. Rev. 442 (2021) 214009.
[14] F. Jiang, B. Ding, S. Liang, et al., Biomaterials 268 (2021) 120545.
[15] L. Wang, L. Mao, F.Y. Qi, et al., Chem. Eng. J. 424 (2021) 130563.
[16] S.Y. Wan, B.Y. Zhang, S. Li, B. He, Y.J. Pu, J. Mater. Chem. B 8 (2020) 4357-4357.
[17] V. Yasothamani, L. Karthikeyan, S. Shyamsivappan, et al., Biomacromolecules 22 (2021) 2472–2490.
[18] L. Wang, Y. He, T. He, et al., Biomaterials 255 (2020) 120208.
[19] S. Zhou, Y. Huang, Y. Chen, et al., Biomaterials 235 (2020) 119795.
[20] F. Ma, J.H. Zhang, J. Zhang, C. Zhang, Cell. Mol. Immunol. 7 (2010) 381–388.
[21] Y. Zhang, G. Zhang, G. Wang, et al., Wiley Interdiscip. Rev. Nanomed. Nanobiotechnol. 13 (2021) e1717.

[22] M.K. Shim, S.K. Song, S.I. Jeon, K.Y. Hwang, K. Kim, Expert Opin. Drug Deliv. 19 (2022) 641–652.
[23] Q. Chen, T. Sun, C. Jiang, Nano Micro Lett. 13 (2021) 92.
[24] H. Ito, T. Ando, Y. Arioka, K. Saito, M. Seishima, Immunology 144 (2015) 621–630.
[25] J.J. Havel, D. Chowell, T.A. Chan, Nat. Rev. Cancer 19 (2019) 133–150.
[26] Y.T. Liu, Z.J. Sun, Theranostics 11 (2021) 5365–5386.
[27] H. Zhang, J. Zhang, Q. Li, et al., Biomaterials 245 (2020) 119983.
[28] L. Han, Y. Zhang, X.W. Chen, Y. Shu, J.H. Wang, J. Mater. Chem. B 4 (2016) 105–112.
[29] Z. Yang, P. Li, Y. Chen, et al., Int. J. Biol. Macromol. 167 (2021) 46–58.
[30] Z. Yuan, C.C. Lin, Y. He, et al., ACS Nano 14 (2020) 3546–3562.
[31] Z.T. Cao, L.Q. Gan, W. Jiang, et al., ACS Nano 14 (2020) 3563–3575.
[32] A.K. Sharma, L. Gupta, H. Sahu, et al., Pharm. Res. 35 (2018) 9.
[33] C. Li, X. Zhang, Q. Chen, et al., ACS Appl. Mater. Interfaces 10 (2018) 2874–2889.